Al-Azhar Bulletin of Science, Section D, Vol. 33, No. 2 (December) 2022, pp. 127-yy
http://doi.10.21608/absb.2022.135621.1180

Al-Azhar Bulletin of Science: Section D

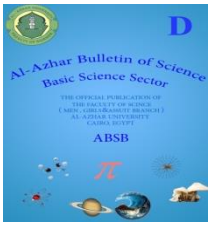

APPLICATION OF WELL LOG ANALYSIS TO ESTIMATE THE PETROPHYSICAL PARAMETERS OF THE LOWER RUDEIS FORMATION IN JULY OILFIELD, GULF OF SUEZ, EGYPT

Moataz Kh. Barakat [a,*], Nader H. EL-Gendy [a], Ahmed M. EL-Shishtawy [a], & Fouad M. Shawaf [b]

[a] Geology Department, Faculty of Science, Tanta University, Tanta, 31527, Egypt.

[b] Exploration Department, Geological Operations and Petrophysics Division, GUPCO, Egypt.
* Corresponding Author: moatazbarakat@science.tanta.edu.eg, moatazbarakat@yahoo.com

Received: 24 Apr 2022; Revised: 08 May 2022; Accepted: 09 May 2022; Published: 01 Dec 2022

ABSTRACT

The Gulf of Suez is considered as a multi-reservoir's basin, containing several reservoirs. It is located at the northeast end of the African plate, along the African-Arab plates. One of the main reservoirs in the Gulf of Suez is the Lower Rudeis (July Member), especially in July Oilfield, and was deposited during the Early Miocene. Comprehensive studies were performed to illustrate the relationships between the different reservoir parameters measured through the well log analysis. The July member reservoir was divided into three zones based on geophysical log responses: denominate zones (A), (B) and zone (C). Petrophysical parameters were calculated, together with lithology and porosity identification cross-plots, for each zone individually to evaluate the July member sandstones. The obtained data indicated that the July member appears to be a good quality reservoir with relatively high storage capacity, with average shale volume of 8 to 42%, average effective porosity of 9.2 to 15.9 %, average calculated permeability of 16.2 to 71 mD, and average hydrocarbon saturation of 10.3 to 73.3 %. The reservoir parameters when mapped at the three levels of the reservoir zones have provided a clear figure about the horizontal distribution of these parameters in the study area and helped in tracing these parameters vertically.

***Keywords*:** Reservoir characterization; July field; July Member; Gulf of Suez; Egypt.

1. Introduction

The Gulf of Suez is a rift basin oriented approximately NNW – SSE; it is approximately 400 km long and varies in width between 40 km and 80 km. The southern end of the Gulf meets the Red Sea which bifurcates into the Gulf of Suez and the Gulf of Aqaba. The Gulf of Suez is considered as a multi-reservoir's basin, containing several reservoirs that range in age from Precambrian to Quaternary [1,2,3]. The most common productive lithology in the Gulf of Suez is sandstone reservoirs besides minor productions from carbonates and fractured basement rocks.

The July oilfield is a complex structural block that is surrounded by normal faults. It is a multi-reservoir oil field in the Gulf of Suez's centre region and is delineated by latitudes 28° 13′ and 28° 18′ to the north, and longitudes 33° 11′ and 33° 17′ to the east [4,5,6,7,8]. July member sandstone is one of the main reservoirs found in the central part of the Gulf of Suez, specifically in the July oilfield, and it was deposited during the Early Miocene (Burdigalian) [9].

In 1973, the July oilfield was found, and production commenced in 1974. A total of 100 wells, including exploration, development, and water injection wells, have been drilled in the July oilfield by the end of 2014. Initial estimates of recoverable reserves of 35 BBO were optimistic since the field had produced about 620 MMBO by the end of 2000. July-58 is a platform in the northern part of the July oilfield. The permitted four wells (July 58-74, July 58-82, July 58-85, and July 58-87) which have been selected in this study (Figure 1).

The main target of this study was to apply petrophysical techniques on July member sandstones to determine the petrophysical

parameters of reservoir in the July oilfield's northern area and the enhanced reservoir characterization which should be taken into consideration in future development.

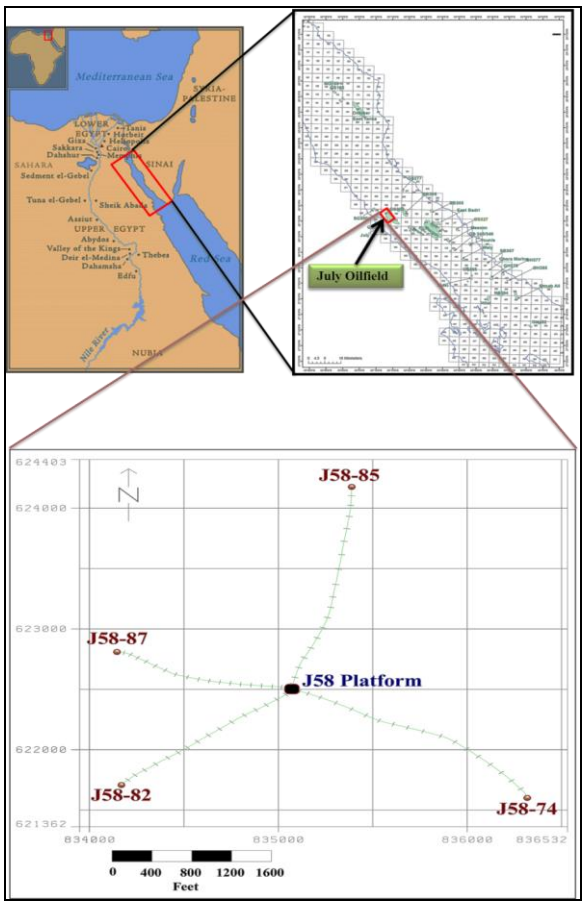

Figure 1. Location map of the July Oilfield.

2. Geological Setting

The Gulf of Suez is a multi-reservoir basin with reservoirs dating from the Precambrian to the Quaternary. It runs in a northwest-southeast direction and forms an elongated graben measuring about 320 km in length, with water depth only 40 - 60 m [7,8,9,10]. The Gulf of Suez rift is a prolonged graben formed by Oligocene rifting that runs north of the Red Sea. The July oilfield is located in Belayim province [13,14].

The three structural provinces (The Northern, Central, and Southern Provinces) of the Gulf of Suez are separated, based on structural setting and regional dip direction the northern and the southern dip SW, while the central dip NE (Figure 2), by two accommodation zones: Zaafrana in the north and Morgan in the south [5,15,16,17,18].

Several authors have divided the stratigraphy section of Gulf of Suez into pre-rift, syn-rift and post-rift (post-Miocene) intervals [5,19,20,21]. Figure (3) illustrates the general stratigraphic section of the July oilfield. Miocene clastic deposits (Rudeis and Nukhul formations), pre-Miocene Cretaceous Nezzazat Group, and Nubia Formation are the major reservoirs of the July oilfield. [2,13,22,23].

3. Materials and Methods

The available four wells (July 58-74, July 58-82, July 58-85, and July 58-87) which have been selected in this study were used for investigating July member clastic reservoir, to evaluate the hydrocarbon potentiality in the study area (Figure1). The open hole 1og data including the traditional tools such as resistivity logs, shallow and deep, neutron, density, sonic and gamma ray for the studied units were collected and digitized. Techlog™ (Version 2015.3) of Schlumberger Inc. was used to perform qualitative and quantitative evaluations for this research.

Each of the four wells used in this study has a log-package composed of gamma ray log (GR), Caliper log (CALI), compressional sonic log (DT), Neutron porosity log (NPHI), Bulk density log (RHOB), Resistivity logs (ILD and ILM).

The lithological and mineralogical components of the July member reservoir was shown using cross-plots. Using gamma ray and neutron density logs, the shale content was determined. After applying different adjustments, the total and effective porosities were calculated using a combination of density neutron and sonic logs. [24,25,26,27]. Formation water resistivity (Rw) also was estimated based on water salinity of actual samples collected from the wells study [28].

On the other hand, effective water saturation was computed using Indonesia [28] methods, and consequently hydrocarbon saturation was estimated.

The obtained July member reservoir properties were mapped to investigate their lateral variation and distribution all over the northern area of July oilfield. To trace the reservoir properties vertically, July member reservoir in the study area was initially subdivided into three zones based on the log responses [30,31]. These subdivisions were used while studying the depositional environment of the July reservoir [32]. July member reservoir subdivisions are called as (A; B; and C) zones, zone A is sandstone with shale while B and C zones have the same lithology as shown in (Table 1). The Shale twenty subzone was separated from zone (A) to eliminate the effect of

the high shale content of this body on the obtained results of zone (A).

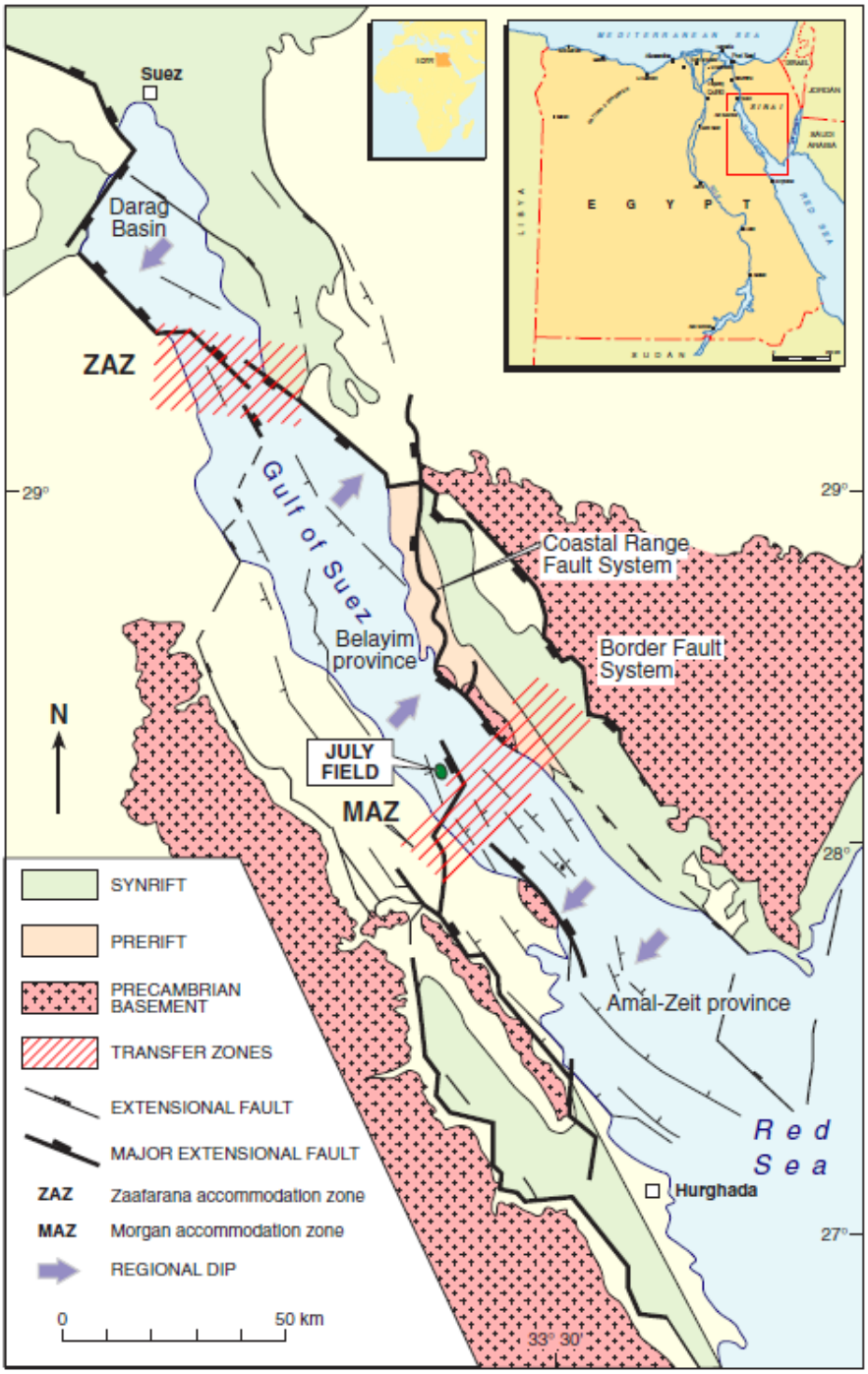

Figure 2. Tectonic elements of the Gulf of Suez, showing the location of the July oilfield [12].

4. Results and Discussions

4.1. Well Logs Correlation

The petrophysical assessment was carried out by analyzing the well logging curves. The purpose of petrophysical analysis was to identify the critical parameters required for reservoir characterization and hydrocarbon potentiality [33]. Because of the massive nature of the sand and the lack of consistent markers, correlation within the July member (Lower Rudeis) has always been difficult and contentious [14,32]. The internal details of the gamma ray log of the July member interval in the study area can be used to divide this interval into three zones, namely zone A, zone B, and zone C, from bottom to top as shown in Figure (4).

4.2. Cross-plot Interpretation

4.2.1. Density-Neutron Cross-Plot

The Density-Neutron Cross-Plot is not only useful in determining the mineralogical composition of a reservoir, but also in estimating the reservoir porosity, in addition to providing good indicators for the reservoir gas content [34].

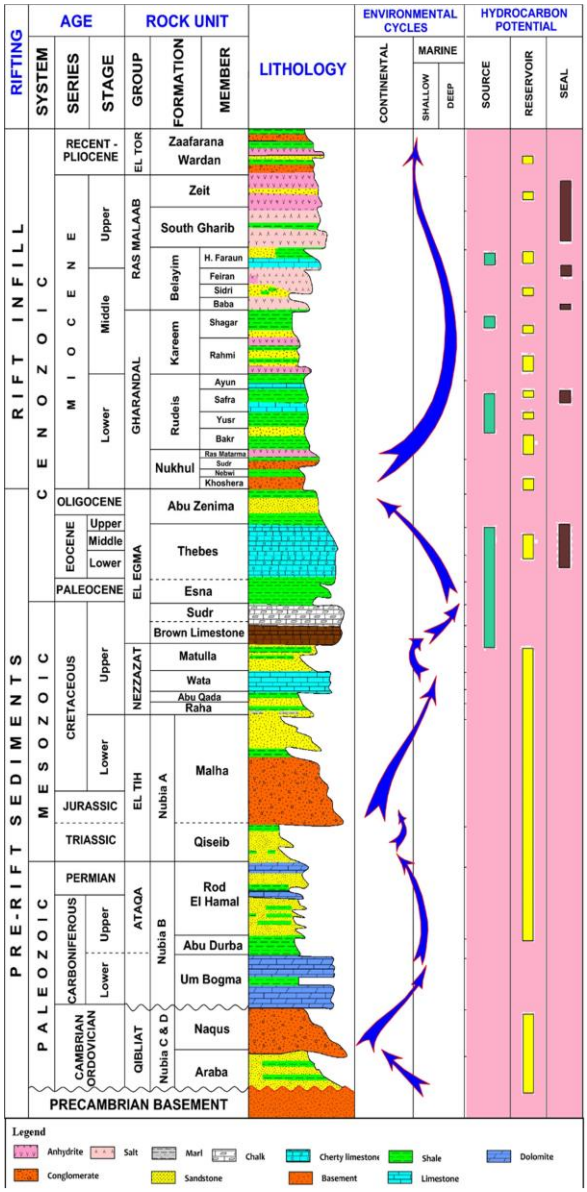

Figure 3. Generalized stratigraphic column of the July oilfield [3].

The shale beds in the four investigated wells of July member reservoir were eliminated; other reservoir intervals were selected accurately and plotted on the density-neutron cross-plot for each zone of the reservoir zones separately (Figure 5). In July 58-74 well, the lithology of this zone (A) is calcareous sandstones with minor traces of its points fell in the pure quartz sandstone line with some shale and the lithology of this zone (B) is mainly calcareous sandstones, with considerable intervals composed of quartz sandstones, while most of zone (C) points appeared to be quartz sandstones with some intervals interpreted as calcareous sandstones. The lithology composition and the porosity determined from the density-neutron cross-plot are indicated in Table 1.

4.2.2. Density-Sonic Cross-Plot

The Density-Sonic Cross-Plot was generated by plotting the bulk density values on Y-axis versus interval transit time values on X-axis. The neutron-sonic cross-plots is considered the most widely used porosity log combination [31]. These cross-plots were achieved for The Lower Rudeis (July Member) zone (A, B, and C) in the studied wells (Figure 6A). In July 58-82 well, the lithology of this zone (A and B) is mostly quartz sandstones with some intervals of calcareous sandstones in addition to some points are referring to dolomitic limestone. While Zone (C) is interpreted as quartz and calcareous sandstones. It worth to mention that points of this well show very high anomalies and randomly scattered behaviour (Figure 6B); this could be attributed to intervals which are highly cemented with different types of cement (i.e; calcite, clay minerals, dolomite, etc.). All the wells' results are presented in Table (1).

4.2.3. MID plot (Matrix Identification plot)

Density, neutron, and sonic logs were used to calculate the apparent matrix density and the apparent matrix interval transit time for July member selected zones in the four investigated wells. The MID plot is generated by plotting the apparent matrix density on Y-axis and the apparent transit time on X-axis over.

Apparent matrix density and apparent matrix transit time are being calculated based on the following equations:

$$\rho_{maa} = \rho_b - (\Phi_{ND} * \rho_f) / 1 - \Phi_{ND} \quad (1)$$

$$\Delta t_{maa} = \Delta_t - (\Phi_{NS} * \rho_f) / 1 - \Phi_{NS} \quad (2)$$

Where: ρ_{maa} is Apparent matrix density, Δt_{maa} is Apparent matrix interval transit time, ρ_b is Density of the matrix, ρ_f is Density of the fluid, Δ_t is Interval transit time from sonic log, Δ_{tf} is Interval transit time of fluid, Φ_{ND} is Neutron-density porosity, Φ_{SN} is Sonic-neutron porosity. The standard matrix identification plot (MID plot) has revealed the following:

Most points of the July member reservoir fell in the area between calcite and quartz but with variable percentages for each zone in the four study wells. This likely indicate that the July

member reservoir contains calcareous sandstones intervals and alternated with quartz sandstones intervals (Figure 7). Points of zone (C) in July 58-74 well showed some deviation perhaps indicating highly cemented intervals (Figure 7A). The scattered plot of points in July 58-82 well likely indicate different types of cementations (calcite, clay minerals, dolomite, etc (Figure 7B). Scattered pattern of points in July 58-85 well could be attributed to the uncertainty in the density and neutron values which were recorded in highly washed-out intervals (Figure 7C).

Table 1: The lithology composition and the porosity determined from the density-neutron and density-sonic cross-plots.

Well	Zones	Density-Neutron Cross-plot			Density-Sonic Cross-plot		
		Lithology	Porosity	Fig.	Lithology	Porosity	Fig.
July 58-74	Zone (A)	calcareous sandstones	3.5 to 17 %	(5A)	calcareous sandstones with some intervals of quartz sandstones	8 to 21 %	(6A)
	Zone (B)	quartz sandstones	3 to 18 %		quartz to calcareous sandstones	9 to 22 %	
	Zone (C)	quartz sandstones with some intervals as calcareous sandstones	4 to 16 %		three different lithology	12 to 20 %	
July 58-82	Zone (A)	pure quartz sandstone	3.5 to 17 %	(5B)	quartz sandstones	10 to 23 %	(6B)
	Zone (B)	quartz sandstones with some intervals calcareous sandstones	5 to17 %		quartz sandstones with calcareous limestones	10 to 25 %	
	Zone (C)	calcareous sandstones	10.5 to 18 %		quartz and calcareous sandstones	16 to 20 %	
July 58-85	Zone (A)	calcareous sandstones	9 to 33 %	(5C)	calcareous sandstones to sandy limestone	14 to 18 %	(6C)
	Zone (B)	calcareous sandstones and quartz sandstones	2 to 31 %		between quartz sandstones and calcareous sandstones	8 to 20 %	
	Zone (C)	calcareous sandstones	5 to 31 %		quartz and calcareous sandstones	10 to 20 %	
July 58-87	Zone (A)	mainly calcareous sandstones	2 to 17 %	(5D)	mostly calcareous sandstones	8 to 18 %	(6D)
	Zone (B)	quartz sandstones and less points as dolomitic limestone	8 to 27 %		quartz sandstones and calcareous sandstones	10 to 25 %	
	Zone (C)	calcareous sandstones	6 to 23 %		calcareous sandstones	12 to 20 %	

4.3. Quantitative Evaluation

4.3.1. Shale Volume Calculations

Gamma ray, neutron and density logs were used to calculate the shale volume of July member reservoir zones in each of the four investigated wells individually. The volume of shale has been calculated using the following equations

$$V_{shale} = GR_{index} \quad (3)$$

$$GRindex = \frac{GRlog - GRmin}{GRmax - GRmin} \quad (4)$$

Where: GR_{log} is Gamma ray log reading (API), GR_{min} is Minimum gamma ray log reading in clean zone (API), GR_{max} is Maximum gamma ray log reading in shale (API).

Clavier method

$$Vsh = 1.7 - \sqrt{3.38\,(GRindex + 0.7)^2} \quad (5)$$

Larionov Tertiary rocks method

$$Vsh = 0.083 \times (2^{(3.7 \times GRindex)} - 1) \quad (6)$$

Comparing the obtained results has revealed that the shale volume calculated using gamma ray log is more or less reliable than that calculated using neutron-density logs, this could be attributed to the variable mineralogical composition of July member reservoir which affected the readings of neutron and density logs [23,32,35,36].

Figure (8) is illustrating the calculated data of the shale volume for different zones of July member reservoir in July 58-74 well where the shale volume cut-off is 30 %.

Table 2: Total and effective porosity results of July member reservoir in the study wells.

Wells	Zones	Values	ΦT_D	Wyllie ΦT_S RHG	ΦT_{NS}	ΦT_{ND}	ΦE_D	ΦE_S RHG	ΦE_{NS}	ΦE_{ND}
July 58-74	Zone (C)	Avg.	0.115	0.095	0.104	0.095	0.081	0.091	0.101	0.091
		Max.	0.174	0.247	0.173	0.150	0.151	0.194	0.159	0.147
	Zone (B)	Avg.	0.132	0.116	0.114	0.120	0.120	0.106	0.100	0.111
		Max.	0.203	0.164	0.160	0.180	0.198	0.159	0.151	0.176
	Zone (A)	Avg.	0.124	0.123	0.115	0.110	0.112	0.108	0.096	0.097
		Max.	0.190	0.193	0.173	0.171	0.189	0.187	0.159	0.165
July 58-82	Zone (C)	Avg.	0.150	0.142	0.136	0.164	0.144	0.124	0.119	0.150
		Max.	0.205	0.222	0.176	0.210	0.199	0.216	0.166	0.199
	Zone (B)	Avg.	0.175	0.133	0.130	0.168	0.171	0.122	0.118	0.159
		Max.	0.222	0.194	0.178	0.211	0.220	0.192	0.163	0.205
	Zone (A)	Avg.	0.146	0.092	0.116	0.135	0.140	0.083	0.103	0.124
		Max.	0.241	0.224	0.174	0.216	0.240	0.220	0.169	0.214
July 58-85	Zone (C)	Avg.	0.140	0.162	0.112	0.130	0.121	0.130	0.109	0.121
		Max.	0.255	0.363	0.281	0.257	0.198	0.277	0.216	0.232
	Zone (B)	Avg.	0.112	0.209	0.104	0.106	0.100	0.194	0.083	0.102
		Max.	0.183	0.283	0.169	0.210	0.179	0.260	0.147	0.202
	Zone (A)	Avg.	0.166	0.235	0.150	0.158	0.134	0.164	0.123	0.121
		Max.	0.239	0.372	0.272	0.253	0.204	0.328	0.256	0.243
July 58-87	Zone (C)	Avg.	0.167	0.126	0.077	0.145	0.157	0.118	0.062	0.139
		Max.	0.231	0.178	0.106	0.215	0.229	0.176	0.099	0.213
	Zone (B)	Avg.	0.169	0.152	0.112	0.154	0.162	0.144	0.107	0.149
		Max.	0.234	0.210	0.186	0.213	0.232	0.206	0.182	0.212
	Zone (A)	Avg.	0.119	0.104	0.098	0.098	0.111	0.098	0.093	0.092
		Max.	0.182	0.173	0.158	0.166	0.179	0.167	0.149	0.159

Table 3: Results of water and hydrocarbon saturation in different zones of July member reservoir in the studied wells.

Wells	Zones	Values	S_w	Hs
July 58-74	Zone (C)	Min.	0.427	0.573
		Avg.	0.617	0.383
	Zone (B)	Min.	0.653	0.347
		Avg.	0.897	0.103
	Zone (A)	Min.	0.437	0.563
		Avg.	0.765	0.235
July 58-82	Zone (C)	Min.	0.193	0.807
		Avg.	0.375	0.625
	Zone (B)	Min.	0.160	0.84
		Avg.	0.267	0.733
	Zone (A)	Min.	0.230	0.77
		Avg.	0.425	0.575
July 58-85	Zone (C)	Min.	0.299	0.701
		Avg.	0.623	0.377
	Zone (B)	Min.	0.281	0.719
		Avg.	0.747	0.253
	Zone (A)	Min.	0.259	0.741
		Avg.	0.421	0.579
July 58-87	Zone (C)	Min.	0.258	0.742
		Avg.	0.463	0.537
	Zone (B)	Min.	0.198	0.802
		Avg.	0.704	0.296
	Zone (A)	Min.	0.423	0.577
		Avg.	0.812	0.188

4.3.2. Porosity Calculations

Porosity is one of the most critical parameters in oil industry which depends on exploring and producing hydrocarbons in the pore spaces found in reservoir zones. Neutron, sonic and density are three main types of logs which were widely used for calculating porosity [37,38]. Each log could be used individually or in a combination with another log.

Effective porosity is the ratio of only interconnected pore space to the bulk volume of the rock. The most trusted and reliable effective porosity formula is as the following:

$$\Phi_{eff} = \Phi_{tot} - (V_{cl} \times \Phi_{sh}) \quad (7)$$

Where: Φ_{eff} is Effective Porosity, Φ_{tot} is Total porosity, Φ_{sh} is Neutron porosity in 100% shale, V_{cl} = Volume of clay.

All the methods of porosity calculations that were discussed above were used to calculate the porosity of July member reservoirs in the four selected wells displayed in (Table 2). Figures (9&10) show the Computed total and effective porosity by different methods for different zones of the July member reservoir in July 58-82 well where the porosity cutoff is 10 %.

4.3.3. Formation water resistivity (Rw)

The quantitative use of resistivity log measurements is at the heart of the whole domain of quantitative log interpretation. Rw is the formation water resistivity; the resistivity of the water trapped in the pore spaces of a porous formation. Salinity and temperature are the most important factors affecting formation water resistivity, where Rw decreases with increasing formation water salinity and temperature. Rw can be detected directly from Schlumberger resistivity chart of NaCl water solution equal 0.021(ohm.m) (Figure11).

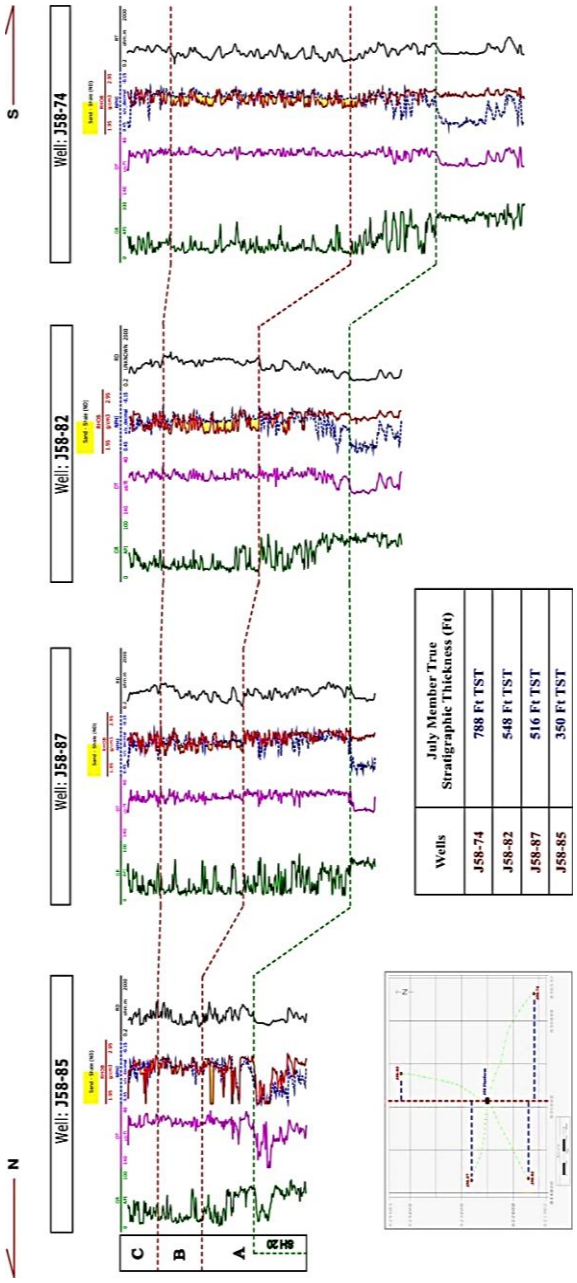

Figure 4. Stratigraphic correlation of July member in July oilfield. The true stratigraphic thickness of July member is decreasing to the north. The correlation is referenced to the base of shale 20 or to the lithological top of Nukhul as a datum. The logs are calibrated to the true stratigraphic thickness are not spaced proportionally to the distances between wells.

4.3.4. Water saturation (Sw)

The hydrocarbon saturation (S_h) is the fraction of the pore volume occupied by hydrocarbons, where ($Sw = 1 - S_h$). water saturation was calculated by Indonesia's method [39] for the July member zones for each well in the study area. This method is used properly to determine the effective water saturation of a reservoir considering the shale volume and shale resistivity an addition to the effective porosity. Indonesia method is considered as more reliable since it reflects reasonable results derived from the analysis of actual log parameters:

$$S_w = \left\{ \left[\left(\frac{V_{sh}{}^{2-V_{sh}}}{R_{sh}} \right)^{\frac{1}{2}} + \left(\frac{\Phi_e{}^{m}}{R_W} \right)^{\frac{1}{2}} \right]^2 \times R_t \right\}^{\frac{-1}{n}} \quad (8)$$

Where: V_{sh} is Voulme of shale, R_{sh} is Resistivity of shale, Φ_e is Effective porosity of the formation, R_t is True formation resistivity. The obtained results were listed in Table (3) for each well in the study area.

4.3.5. Permeability (K)

Permeability can be determined by different methods. El-Gendy et al., (2017) [32] stated that the most applicable method for the July oilfield is the equation introduced by Wyllie and Rose, (1957) [40].

$$K = \left(250 \times \frac{\Phi^3}{S_{Wirr}} \right)^2 \quad (9)$$

The results of permeability for different zones of the July member sandstones in each of the studied wells are listed in Table (4). Figure (12) shows the saturations and permeability layout for different zones of the July member reservoir in July 58-87 well.

Table 4: Permeability results for different zones of July member reservoir in the studied wells.

Wells	Zones	Permeability (mD)		
		Min.	Avg.	Max.
July 58-74	Zone (C)	3.97	24.99	301.90
	Zone (B)	1.58	52.46	255.98
	Zone (A)	1.65	23.78	194.71
July 58-82	Zone (C)	1.28	58.18	383.17
	Zone (B)	5.16	70.92	319.24
	Zone (A)	3.59	48.90	386.29
July 58-85	Zone (C)	6.06	19.74	217.69
	Zone (B)	2.99	16.80	172.70
	Zone (A)	6.42	16.16	170.58
July 58-87	Zone (C)	1.02	53.09	377.88
	Zone (B)	5.21	66.62	370.57
	Zone (A)	2.11	41.34	164.98

4.4. Horizontal Variations of Reservoir Parameters

4.4.1. Shale volume iso-parametric mapping

Shale volume was calculated using several methods in the July member reservoir zones for the four wells of the current study. Final calculated shale volume was mapped at the level of each reservoir zone. The obtained iso-

parametric maps have revealed that, shale volume increases to the northeast direction, towards July 58-85 well and to the southwest direction, towards July 58-82 well (Figure 13).

4.4.2. Effective porosity iso-parametric mapping

Mapping the effective porosity reflects the distribution of the reservoir quality within the study area. The best effective porosity appeared in southwest direction, (Figure14), especially at zone (C) level. However, the magnitude of the effective porosity spreads with depth in both northeast and southwest directions at zone (A) level.

4.4.3. Permeability iso-parametric mapping

At the levels of zone (A) and zone (C), permeability is clearly increasing towards west and southwest directions. At the level of zone (B), permeability has the same behaviour and directions but with greater magnitude. The maximum value of the calculated permeability occurs to the west of July 58-82 and July 58-87 wells at the level of zone (B). Also, at zone (B) level, July 58-74 well has greater permeability than that at the above and below zones (Figure 15).

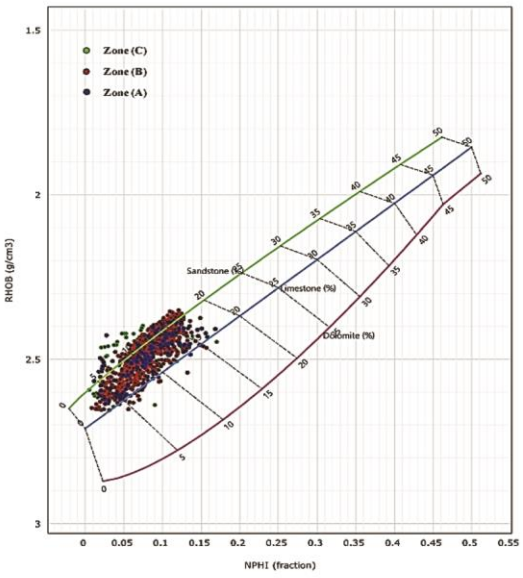

(A) July 58-74 well.

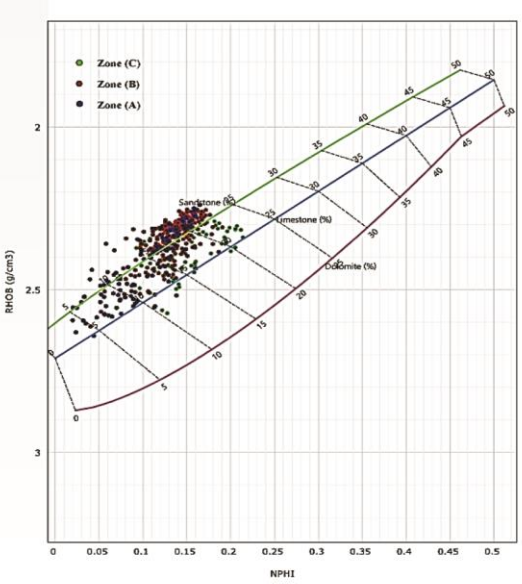

(B) July 58-82 well.

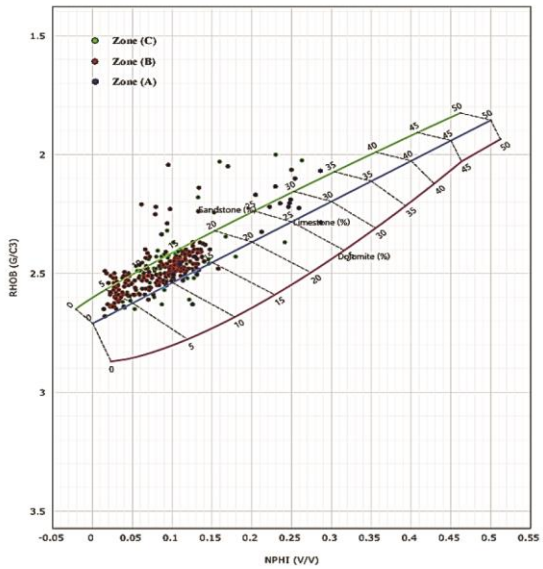

(C) July 58-85 well.

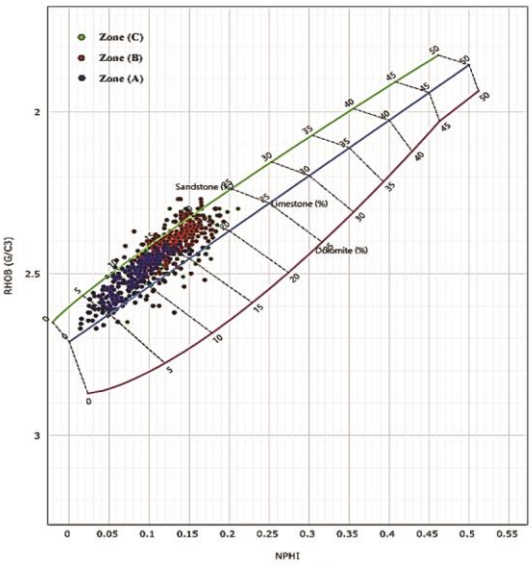

(D) July 58-87 well.

Figure 5. Density-neutron cross-plot for different zones of July member reservoir in the available wells ((A) July 58-74well; (B) July 58-82 well; (C) July 58-85 well; and (D) July 58-87 well)).

4.4.4. Hydrocarbon saturation iso-parametric mapping

Effective hydrocarbon saturation was mapped at different levels of the study area and the obtained iso-parametric maps show the distribution of the hydrocarbon potentiality horizontally and vertically as well. Water saturation reach the maximum values towards the southeast direction (July 58-74 well) at all levels of the reservoir. Conversely, hydrocarbon saturation is confined in the southwest direction (July 58-82 well), at all levels of the reservoir (Figure16).

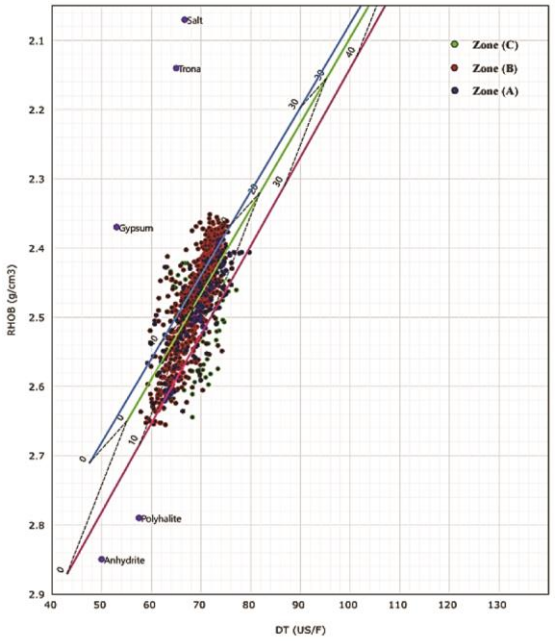

(A) July 58-74 well.

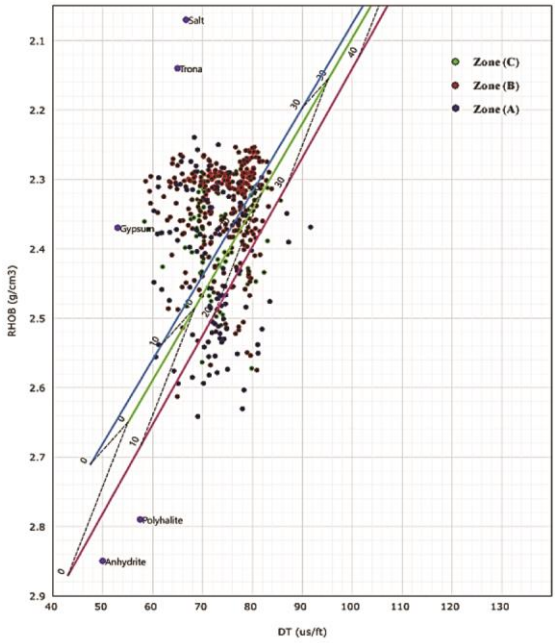

(B) July 58-82 well.

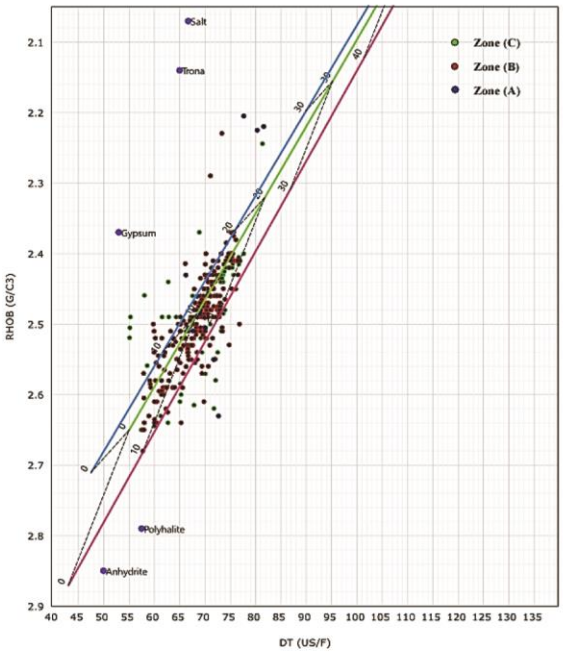

(C) July 58-85 well.

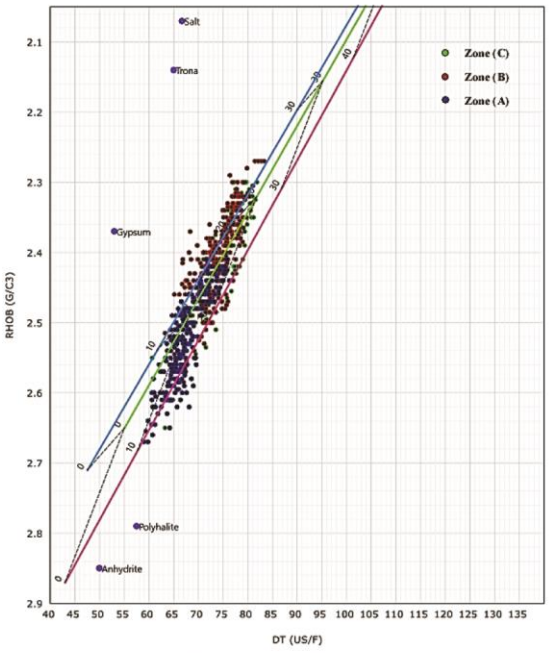

(D) July 58-87 well.

Figure 6. Density-sonic cross-plot for different zones of July member reservoir in the available wells ((A) July 58-74well; (B) July 58-82 well; (C) July 58-85 well; and (D) July 58-87 well)).

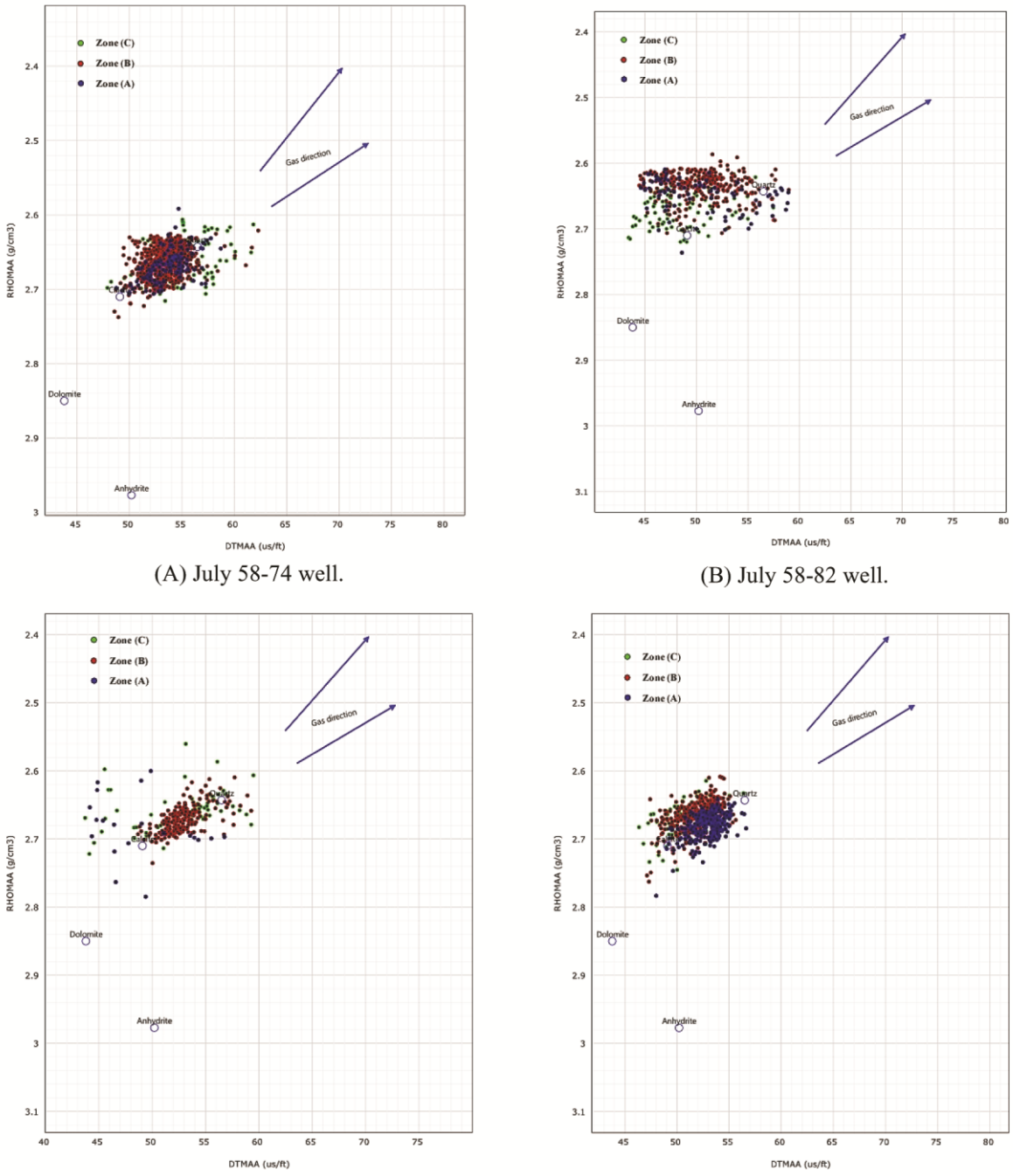

(A) July 58-74 well.

(B) July 58-82 well.

(C) July 58-85 well.

(D) July 58-87 well.

Figure 7. Mid cross-plot for different zones of July member reservoir in the available wells ((A) July 58-74well; (B) July 58-82 well; (C) July 58-85 well; and (D) July 58-87 well).

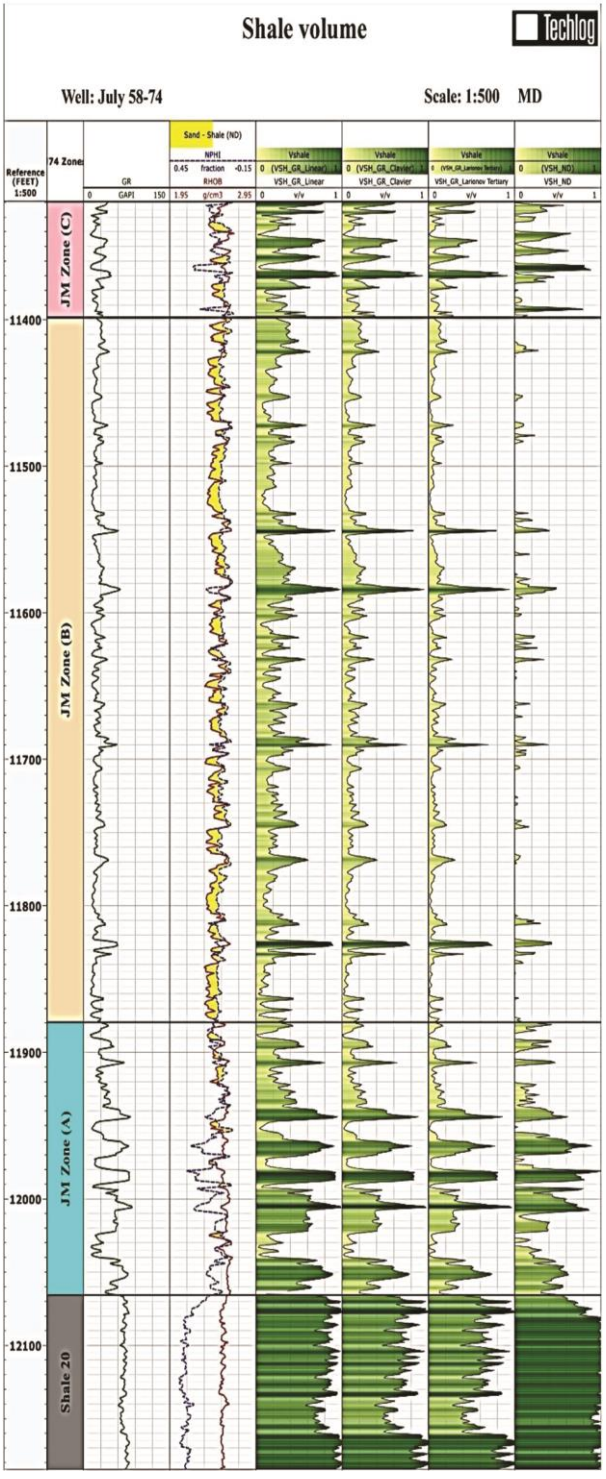

Figure 8. Computed shale volume for different zones of July member reservoir in July 58-74 well.

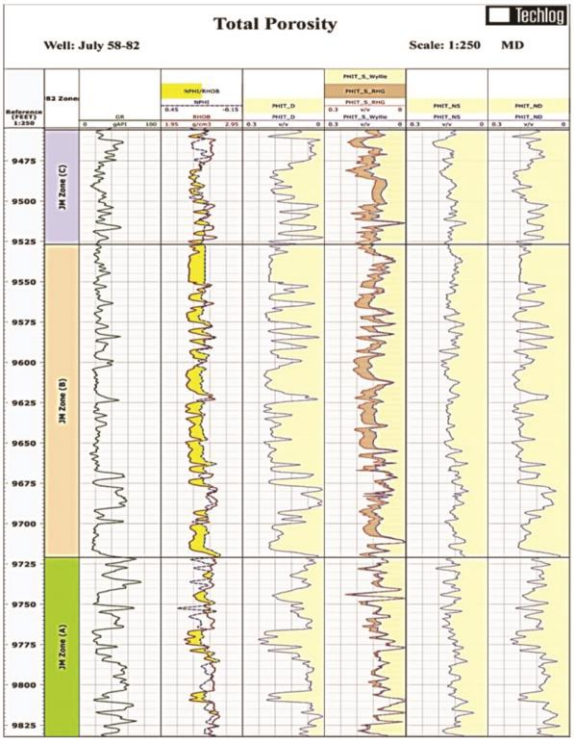

Figure 9. Computed total porosity by different methods for different zones of July member reservoir in July 58-82 well.

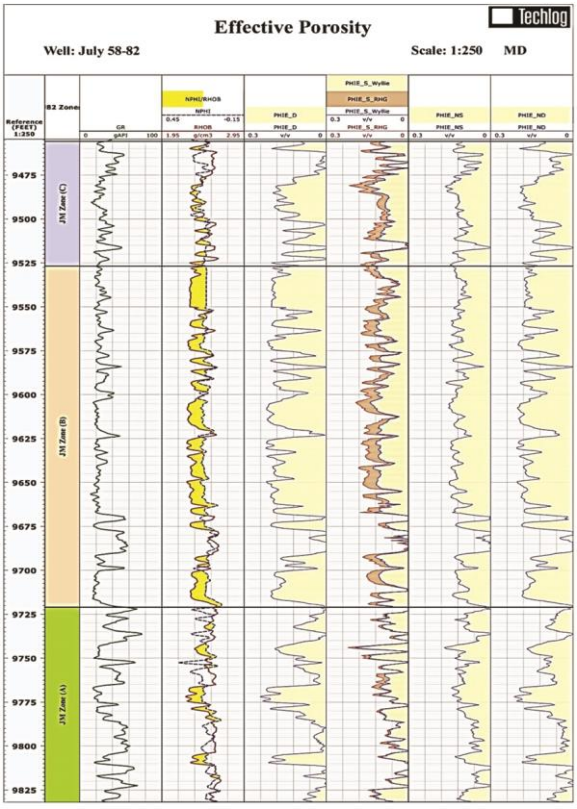

Figure 10. Computed effective porosity by different methods for different zones of July member reservoir in July 58-82 well.

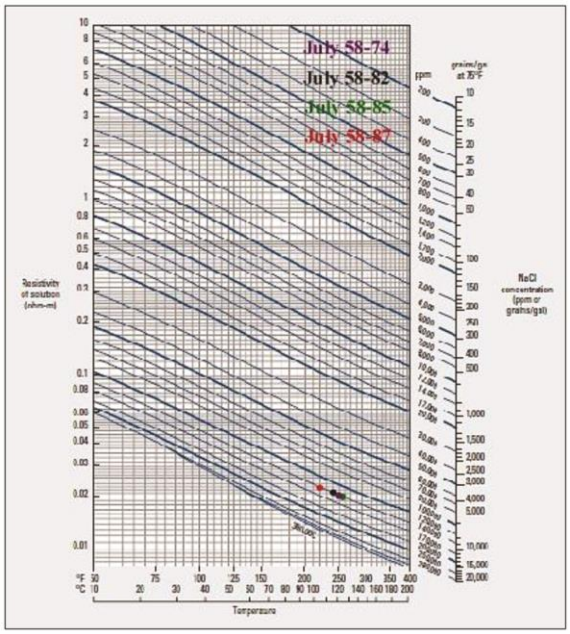

Figure 11. Resistivity chart of NaCl water solution, showing values of formation water resistivity R_w, based salinities and formation temperatures for the four wells of the current study.

5. Conclusions

Petrophysical evaluation of the July member reservoir has been done throughout different techniques to define the required parameters of this reservoir. Cross-plot technique was used to identify lithology and porosity in different zones of the reservoir. The study revealed that the main lithology of the reservoir is calcareous sandstones with some intervals that were identified either as quartz sandstones or as dolomitic sandstones. Geophysical log responses divided the July member reservoir into three zones (A, B, and C). The geothermal gradients in the four investigated wells ranged between 1.52-1.77 °F/100ft mathematically, and between 1.53-1.75°F/100ft, graphically. The total porosity values ranged between 9.6 - 25.7 %, while the effective porosity values ranged between 9.1-25.3 %. And the values of permeability which was calculated in the reservoir zones were between 1.02 and 386.29 mD. Water saturations were calculated using Archie's method and ranged between 17.6 - 96.1 %, whereas the effective water saturation using Indonesia's method ranged between 16.7 - 89.7%. Consequently, the hydrocarbon saturations could be detected in the zone of interest in the study wells. Shale volume is increased horizontally towards northwest direction (July 58-85 well), whereas the effective porosity increased in the opposite direction (southeast direction). On the other hand, hydrocarbon saturation is increasing at all levels of the reservoir towards southeast direction. So, the southeast direction is the best area to exploration development.

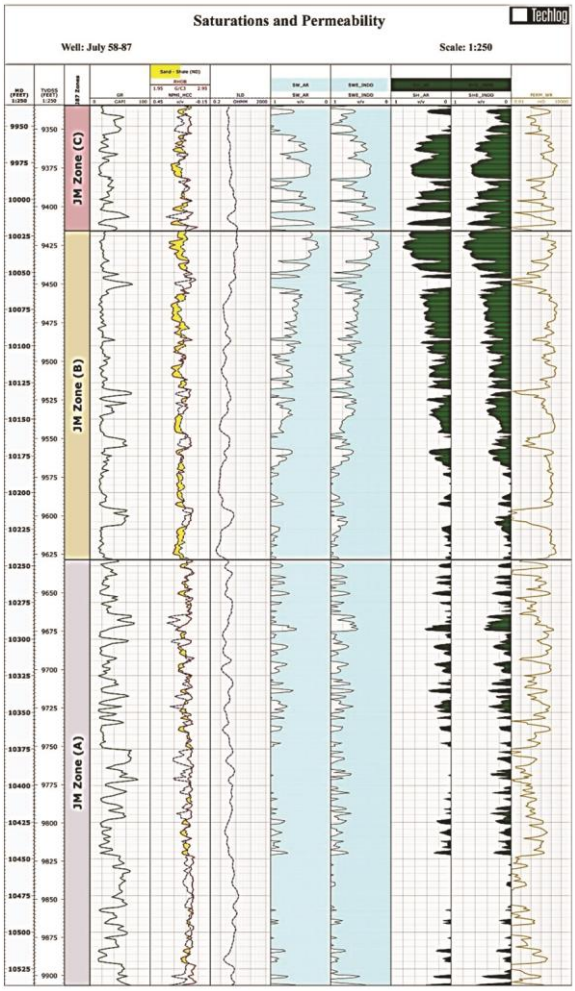

Figure 12. Saturations and permeability layout for different zones of July member reservoir in July 58-87 well.

Funding sources

This research received no external funding.

Conflicts of interest

There are no conflicts to declare.

Acknowledgment

The authors would like to extend their appreciation and acknowledgement to the editor-in-Chief for handling our manuscript. Also, deep thanks to the (EGPC) Egyptian General Petroleum Cooperation and Gulf of Suez Petroleum Company (GUPCO) for providing data for this research.

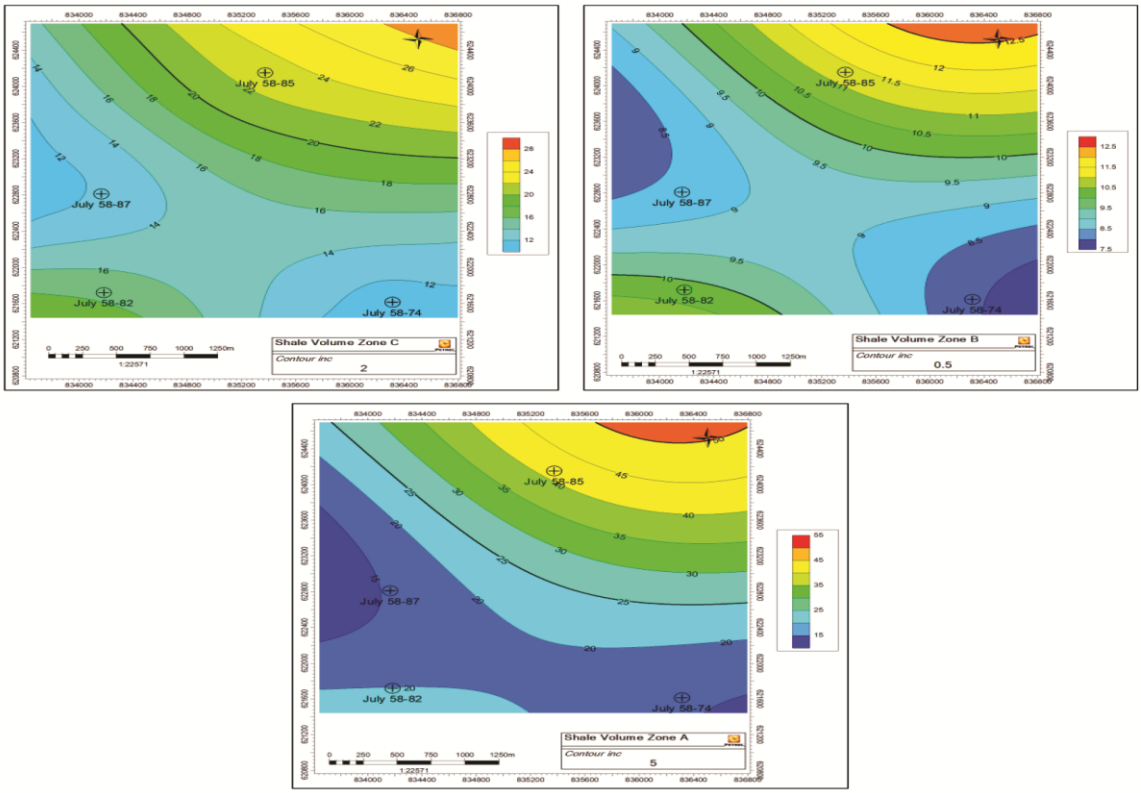

Figure 13. Shale volume horizontal tracing all over the area of study.

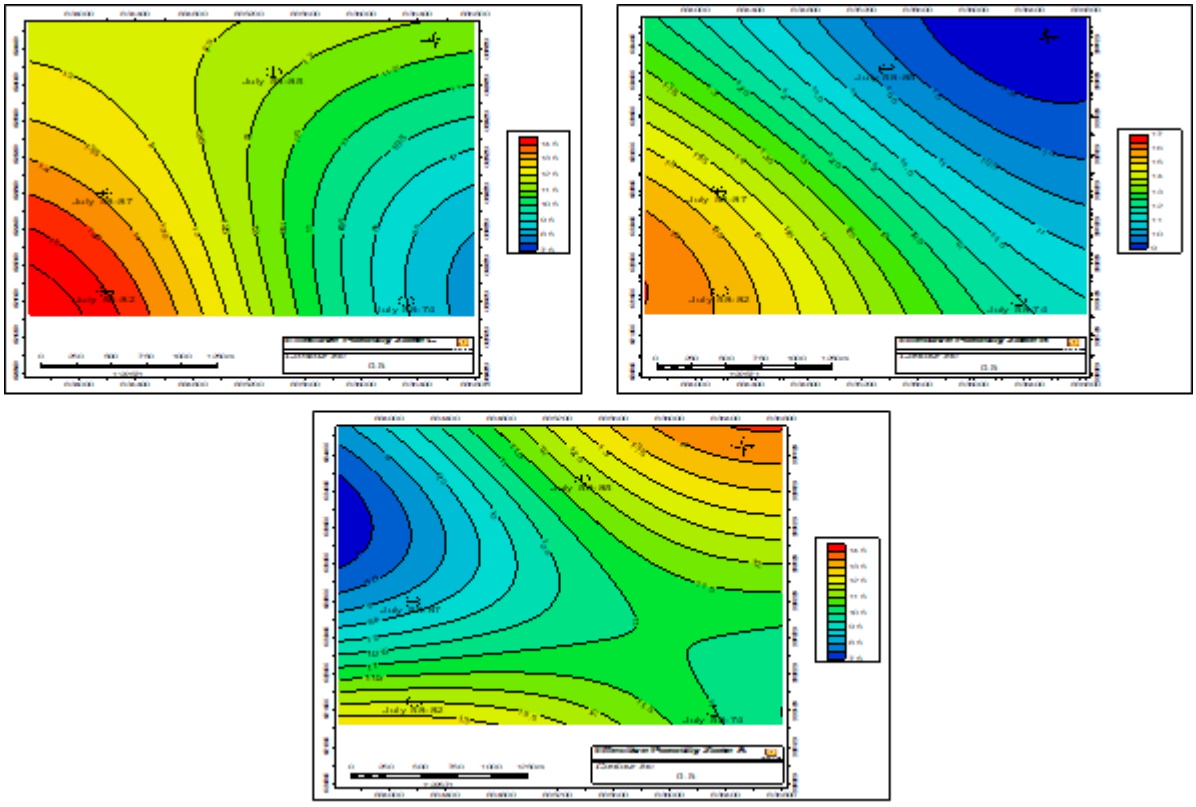

Figure 14. Effective porosity horizontal tracing all over the area of study.

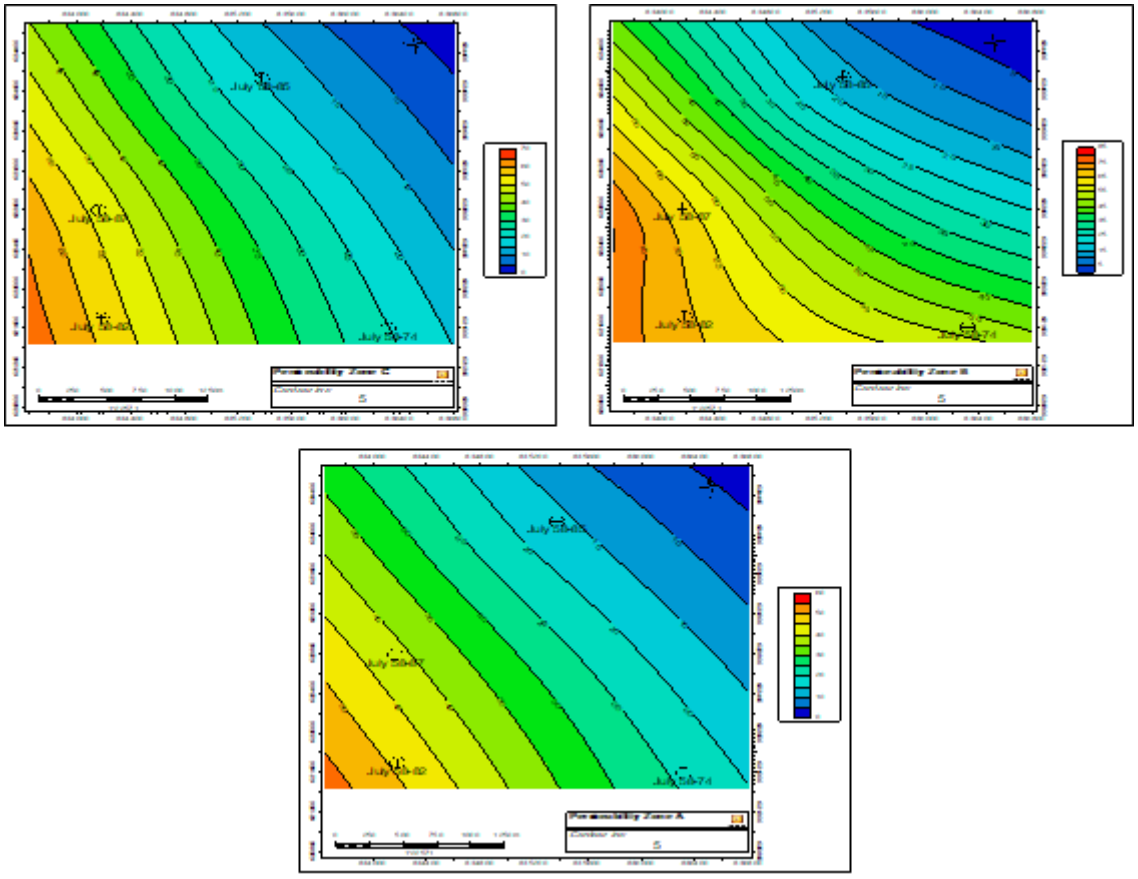

Figure 15. Permeability horizontal tracing all over the area of study.

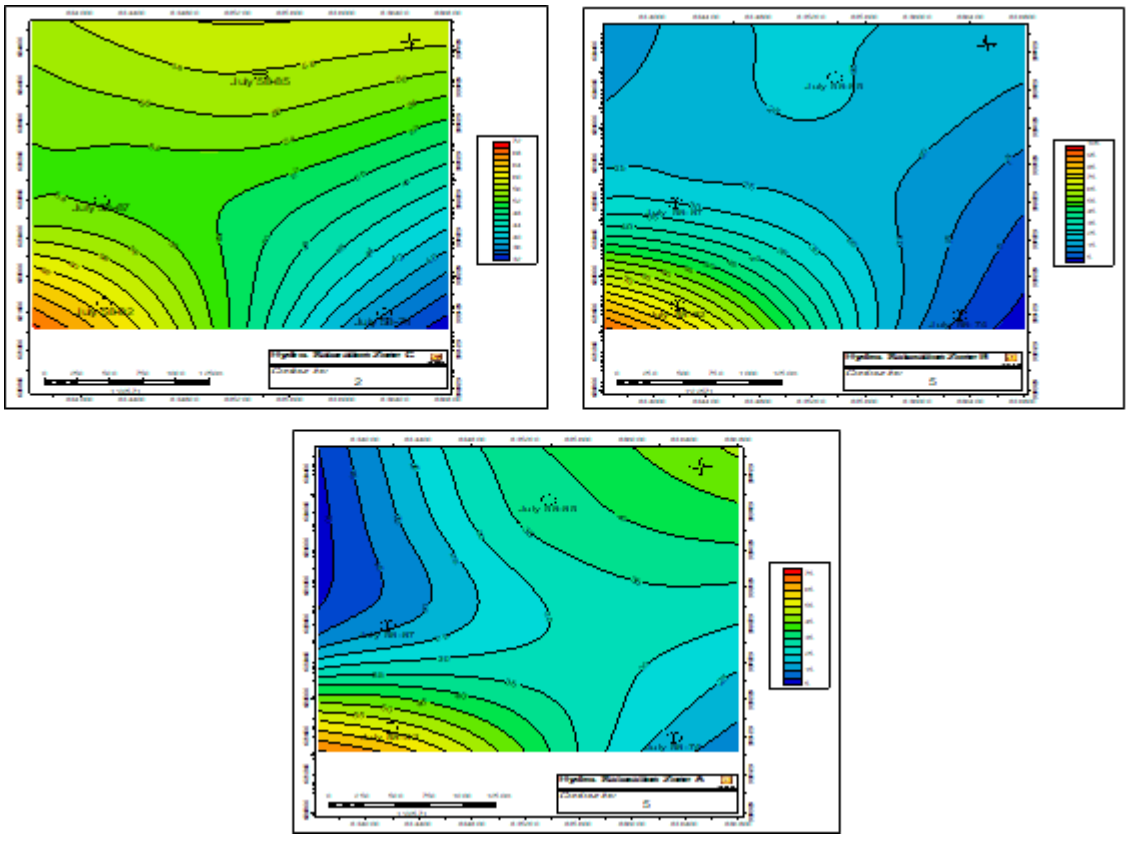

Figure 16. Hydrocarbon saturation horizontal tracing all over the area of study.

References

[1] Said R, The Geology of Egypt, Elsevier, New York;1962. 377 pp.

[2] EGPC, Egyptian General Petroleum Corporation, Nile Delta north Sinai fields, discoveries and hydrocarbon potentialities (as comprehensive overview). EGPC-Cairo, Egypt; 1994.387 pp.

[3] Al-sharhan A S, Salah M G. Geology and hydrocarbon habitat in rift setting: northern and central Gulf of Suez, Egypt. Bulletin of Canadian Petroleum Geology; 1995. 43(2), 156– 176.

[4] Said R, The Geology of Egypt A. Balkema Publishers, USA; 1990. 734 pp.

[5] Darwish M, El Araby A. Petrography and diagenetic aspects of some siliclastic hydrocarbon reservoir in relation to the rifting of the Gulf of Suez, Egypt, Geol. Soc. Egypt Spec. Publ. No1; 1993.p. 155-187.

[6] Wescott WA, Attia M, Dolson JC. A brief history of the exploration history of the Gulf of Suez, Egypt. In: AAPG International Convention and Exhibition, Cancun, Mexico; 6-9 Sept 2016. Search and Discovery Article #30473.

[7] Barakat M Kh. Modern geophysical techniques for constructing a 3D geological model on the Nile Delta, Egypt. PhD Dissertation: Technische Universität Berlin; 2010, p.158.

[8] El-Gendy N, Barakat M, Abdallah H. Reservoir assessment of the Nubian sandstone reservoir in South Central Gulf of Suez, Egypt. Journal of African Earth Sciences, 129; 2017a, pp. 596-609.

[9] Shawaf F, Facies analysis and hydrocarbon evaluation of the Lower Miocene (Rudeis Formation) in July Oilfield, Gulf of Suez, Egypt, Msc. Tanta University; 2017, pp. 295.

[10] Jackson JA, White NJ, Garfunkel Z, Anderson H. Relations between normal-fault geometry, tilting and vertical motions in extensional terrains: an example from the southern Gulf of Suez. J. Struct. Geol. 10; 1988.155–170.

[11] Richardson M, Arthur M A. The Gulf of Suez-northern Red Sea Neogene rift: a quantitative basin analysis. Marine and Petroleum Geology, 5(3);1988. 247-270.

[12] McClay K, Nichols G, Khalil S, Darwish M, Bosworth W. Extensional tectonics and sedimentation, eastern Gulf of Suez, Egypt. In B. H. Purser & D. W. J. Bosence (Eds.), Sedimentation and tectonics of rift basins, Red Sea- Gulf of Aden ;1998. pp. 223–238. Chapman and Hall.

[13] EGPC, Egyptian General Petroleum Corporation, Gulf of Suez oil fields (A comprehensive overview) Cairo, Egypt ;1996. pp. 484-495.

[14] Gaafar G, Attia G, Khaled A, Ibrahim S. pertrophysical Evaluation of Rudeis Reservoir in July Oil Field, Gulf of Suez, Egypt, Second International Conference on the Role of Applied Geology in Environmental Development; 2009. P. 1-21.

[15] Khalil S, McClay K. Structural architecture of the Eastern Margin of the Gulf of Suez: field studies and analogue modelling results. 14th EGPC Conference, Cairo;1998. pp. 201-211.

[16] Younes A I, McClay K. Development of accommodation zones in the Gulf of Suez-Red Sea rift, Egypt. American Association of Petroleum Geologists Bulletin 86; 2002.1003–1026.

[17] Day R A, Hoffman K S. more efficiently taps Suez oil using 3-D modeling. World oil, 218(9); 1997. 47–53.

[18] Abu-Hashish M F, Afify H M. Effect of petrography and diagenesis on the sandstone reservoir quality: a case study of the Middle Miocene Kareem Formation in the North Geisum oil field, Gulf of Suez, Egypt. Arabian Journal of Geosciences; 2022, 15:465. https://doi.org/10.1007/s12517-022-09686-z.

[19] Colletta B, Le Quellec P, Letouzey J, Moretti I. Longitudinal evolution of the Suez Rift Structure (Egypt). Tectonophysics, 153;1988. 221–233.

[20] Kassem A A, Sharaf L M, Baghdady A R, El-Naby A. Cenomanian/Turonian oceanic anoxic event in October oil field, central Gulf of Suez, Egypt. Journal of African Earth Sciences; 2020.165, 103817.

[21] Shehata A A, Kassem A A, Brooks H L, Zuchuat V, Radwan A E. Facies analysis and sequence-stratigraphic control on reservoir architecture: Example from mixed carbonate/siliciclastic sediments of Raha Formation, Gulf of Suez, Egypt. Marine and Petroleum Geology; 2021.131, 105160.

[22] Hosny W A, Gaafar I, Sabour A. Miocene stratigraphic nomenclature in the Gulf of Suez, 8th EGPC Exploration Seminar, Cairo;1986. 10 p.

[23] Ouda K H, Masoud M Sedimentation history and geological evolution of the Gulf of Suez during the Late Oligocene-Miocene, Geol. Soc. Egypt, Spec. Publ. No.1;1993. p.47-88.

[24] Schlumberger, Log interpretation: v. 2 (application). Schlumberger Limited, New York; 1974. p.116.

[25]Dresser Atlas, Log interpretation charts. Houston, Dresser Industries, Inc; 1979. p. 107.

[26]Abdullah EA, Al-Areeq N M Al-Masgari A, Barakat M Kh. Petrophysical evaluation of the Upper Qishn clastic reservoir in Sharyoof oil Field, Sayun-Masilah Basin, Yemen. ARPN Journal of Engineering and Applied Sciences, 16(22); 2021. pp. 2375-2394.

[27]Barakat M Kh, Azab A A, Nabil M. Reservoir Characterization Using the Seismic Reflection Data: Bahariya Formation as a Case Study, Shushan Basin, North Western Desert, Egypt. Journal of Petroleum and Mining Engineering; 2022. 24 (1) p.1-11, 2021.DOI: 10.21608/jpme.2022.110315.1107.

[28]Rider M. The geological interpretation of well log (2nded.). London: Whittles Publishing; 1996. ISBN 9780954190606.

[29] Poupon A, Leveaux J. Evaluation of water saturation in shaly formations. In: Proceedings of the SPWLA 12th annual logging symposium;1971.

[30]Asquith GB, Gibson CR. Basic well log analysis for geologists. American Association of Petroleum Geologists, Tulsa;1997. 215 p.

[31]Asquith G, Krygowski D. Basic well log analysis, (2nded.) AAPG Methods in Exploration, 16: ; 2004.13–35.

[32]El-Gendy N, El-Shishtawy A, Barakat M Kh, Shawaf FM. Applying sedimentological and geophysical techniques for facies analysis and depositional history of July Member sandstones, the northern area of July oilfield, Gulf of Suez-Egypt. IOSR Journal of Applied Geology and Geophysics (IOSR-JAGG ;2017b. pp. 84-106.

[33]Barakat M Kh, Nooh A Z. Reservoir quality using the routine core analysis data of Abu Roash "C" in Badr El Din-15 oil field, Abu Gharadig basin, North Western Desert, Egypt. Journal of African Earth Sciences, 129; 2017. 683-691.

[34]Schlumberger, Log Interpretation Charts. Schlumberger Well Services, New York, USA;1986. pp. 44-45.

[35]Clavier C, Hoyle W R, Meunier D. Quantitative interpretation of TDT logs: parts I and II, J Pet. Tech;1971. pp.743–763.

[36]Dresser Atlas, Well logging and interpretation techniques, the course for home study. Dresser Industries Inc, Houston;1982.

[37]Schlumberger, Well evaluation conference of Egypt. Schlumberger, Middle East;1984. 201 p.

[38]Schlumberger, Log interpretation/charts: Huston, Schlumberger Well Services, Inc.;2006. p. 386.

[39]Simandoux P. Dielectric measurements on porous media: application to the measurement of the water saturations: study of the behaviour of argillaceous formations. Revue De I, institute francais Du Petrol 18, Supplementary Issue, 193–215 (translated text in Shaly Sand Reprint Volume, SPWLA, Houston;1963. pp. 97–124.

[40]Wyllie M R, Rose WD. Some theoretical considerations related to the quantitative evaluation of the physical characteristics of reservoir rocks from electrical log data: Petroleum Transaction of AIME, 189: ;1957.105-118

تطبيق تحليل الرصد البئري لتقدير المعاملات البتروفيزيائية لمتكون روديس السفلي في حقل يوليو النفطي، خليج السويس – مصر

معتز خيري بركات[1]، نادر حسني الجندي[1]، أحمد مصطفي الششتاوي[1]، فؤاد محمود شواف[2]

1. قسم الجيولوجيا، كلية العلوم، جامعة طنطا، طنطا31527 - مصر

2. قسم الاستكشاف ، قسم العمليات الجيولوجية والبتروفيزياء ، جابكو ، مصر

الملخص

يعتبر خليج السويس الذي يقع في الطرف الشمالي الشرقي من القارة الافريقية حوض متعدد الخزانات الصخرية التي يتراوح عمر صخورها ممن قبل الكمبري والعصر الحديث. يهتم هذا العمل البحثي بدراسة الجزء السفلي من متكون روديس والمعروف بعضو يوليو في حقل يوليو النفطي الذي يقع بالجزء الاوسط من خليج السويس بهدف توصيف خصائصها البتروفيزيائية باستخدام بيانات الرصد البئري. يعتبر عضو يوليو الصخري من عصر الميوسين، وهو احد الخزانات الصخرية الرئيسية في خليج السويس ومن دراسة سمات منحنيات الرصد البئري الفيزيائية والمعلومات الجيولوجية المتوفرة امكن تقسيم هذة الوحده الصخرية الي ثلاث نطاقات مختلفة ودل عليها بالرموز أ، ب، ج بدا من اسفل الي اعلي وتم تقييم المعاملات البتروفيزيائية للنطاقات الثلاثة مثل محتوي الطفلة والمسامية والتشبع بالنفط وتم تقديم نتائج التحليل في شكل اعمدة لاظهار توزيعات الخصائص البتروفيزيائية راسيا وفي شكل خرائط وقد تم استخلاص ان خزان يوليو ذات خصائص بتروفيزيائية جيدة وتحتوي علي صخور ذات سعة تخزينية عالية ومليئة بالنفط وان المنطقة الجنوبية الغربية هي الاعلي جودة للخصائص البتروفيزيائية التي يمكن حفر ابار جديدة بها.